The design, synthesis and characterization of a novel acceptor for real time polymerase chain reaction using both computational and experimental approaches

Design, synthesis and characterization of a novel acceptor for a PCR pair by computational and experimental approach.

Caterina Benzi[a*], Chiara A. Bertolino[b], Ivana Miletto[a], Paola Ponzio[b], Claudia Barolo[c], Guido Viscardi[c], Salvatore Coluccia[a], Giuseppe Caputo[a,b]

[a] *Dipartimento di Chimica IFM, Università di Torino, Via P. Giuria 7, 10125 Torino, Italy and NIS Centre of Excellence, Università di Torino, Via P. Giuria 7, 10125 Torino, Italy*

[b] *Cyanine Technologies S.r.l., Via Quarello 11, 10135 Torino, Italy*

[c] *Dipartimento di Chimica Generale e Chimica Organica, Università di Torino, Corso Massimo d'Azeglio 48, 10125 Torino, Italy and NIS Centre of Excellence, Università di Torino, Via P. Giuria 7, 10125 Torino, Italy*

[*] corresponding author: caterina.benzi@unito.it

Keywords: indocyanine, DFT, Time-Dependent DFT, fluorescence quenching, PCR pair, nitro-indocyanine

Abstract

The design of a novel fluorescence acceptor for Real Time Polymerase Chain Reaction analysis has been carried out with the help of in-depth computational analysis of structure/property relationships. A functionalized dye **2** belonging to the indocyanine family has been synthetized with a view to subsequent use as a quencher for a fluorescent cyanine dye **1**. A pentamethine indocyanine has been functionalized with nitro groups in order to enhance quenching properties; *ad hoc* substituents have been used to enable conjugation with DNA strand. The visible absorption and photoemission of **2**

and of a reference unsubstituted indodicarbocyanine dye, taken as model of chromogen system, have been addressed both theoretically and experimentally. A Förster resonance energy transfer test has been simulated experimentally to evaluate the quenching efficiency of the donor/acceptor couple.

Introduction

Real Time Polymerase Chain Reaction (PCR) is a widely applied technique in diagnostics, which allows the DNA amplification process to be monitored quantitatively. For such an application it is fundamental to couple a fluorescent donor dye and an acceptor/quencher dye on the two sides of the same oligonucleotide [1,4]. When the probe is intact, the proximity of the quencher greatly reduces the fluorescence emitted by the donor dye, as the absorption of light by the latter molecular species promotes electronic excitation in the acceptor molecules; the excited acceptor subsequently decays either by fluorescence or by other means, such as vibrational dissipation. This phenomenon is known as resonance energy transfer (RET) [5] and occurs in chemical systems comprising two (or more) chromophores with absorption and fluorescence bands at similar, but experimentally differentiable, wavelengths. The rate of energy transfer is thus proportional to the spectral overlap of the emission and absorption bands of the donor and acceptor molecules, respectively. On the other hand, the absorption wavelengths of the two dyes need to differ, in order to excite only the donor. Otherwise, the recorded emission will not be the direct measurement of the energy transfer only. The structure of the dyes is fundamental for an efficient energy transfer and the ease of bioconjugation with the biological system. The quest for new and better performing fluorophore/quencher pairs leads to an in-depth physico-chemical study of the properties of organic dyes.

In recent years, cyanine dyes have been used as fluorescent probes for biomedical screening techniques [6]. These dyes can be easily used in biological applications because of their absorption and fluorescence characteristics. Their large fluorescence spectrum range and good fluorescence

quantum yield enable the detection of very low concentrations of analytes. For specific applications in the field of Real Time PCR, cyanine dyes are already widely used as the donor [7] as they appear to be effective for the various emission wavelengths they can offer. Moreover, they can also be employed as FRET acceptors [8-10], considering that their structural flexibility [11] allows modification of their absorption and emission properties, in such a way it is possible to improve the energy transfer between donor and acceptor and reduce the background noise during Real-Time PCR experiments.

Recently some examples of quenchers based on cyanine dye structure have been reported [12,13]. In the former reference, a di(sulfonatoalkyl)amino indolenine is used to synthesize non fluorescent cyanine dyes. In the latter reference, luminescence quenching moieties are covalently linked to cyanine dyes in various positions. These luminescence quenching groups are heterocyclic compounds, among which thiophene, pyrrole and indole and may be substituted with nitro groups. We believe that also indocarbocyanine dyes containing nitro groups conjugated to the chromogen may act as quenchers: in fact, the presence of the nitro group on aromatic systems is effective in reducing the emission features of many organic compounds [14].

Trimethine-indocarbocyanine/pentamethine-indocarbocyanine donor-acceptor fluorophore pair is a popular choice in single-molecule fluorescence studies [7 and references within]. Dye **1** [15] (Scheme 1) is a water-soluble trimethine-indocarbocyanine dye functionalized for bioconjugation and suitable for PCR analysis, similarly to the commercial analogue Cy3.5 [16]. In this paper, we present a modified pentamethine-indocarbocyanine (dye **2**, Scheme 1) appropriately designed as an acceptor species in a RET couple with the previous molecule. The indocarbocyanine skeleton has been functionalized with one nitro groups on each indole ring and with functionalized alkyl spacer arms for the bioconiugation with nucleotides (Scheme 1).

Please, insert here Scheme 1.

The design of this new dye and the prediction of molecular properties takes advantage of a theoretical approach which is able to rationalize the structure/property relationship and helps the structural characterization in a joint approach with experimental chemical-physical techniques. An obstacle to an in – depth analysis of absorption and emission spectra of variously functionalized cyanines is the size of the molecular system. A very powerful tool, suitable to study large molecules of practical interest, is rooted in the Density Functional Theory (DFT) [17]. In the past years, such methods have been successfully used for structural determination and property calculation of organic molecules. In recent years, DFT has also been extended to excited states, and Time-Dependent Density Functional Theory (TD-DFT) [18,19] for the calculation of excited state energies and oscillator strengths of molecules has been implemented in several quantum chemical packages. Cyanine dyes have been an interesting benchmark for testing the efficiency of various computational methods in describing the properties of optically active molecules [20-23]. However, most of the theoretical studies have dealt with open-chain polymethine dyes or with thiocarbocyanines; very few studies have been reported on the investigation of emission properties [24] and structure/fluorescence relationship [25,26] and to our knowledge, only one previous paper, investigating solvatochromic effects, is focused on indocyanines [27].

In this work, a DFT based computational approach was employed to design the new dye **2**. The absorption and emission wavelengths of dye **1** were also calculated to evaluate the overlap between donor emission and acceptor absorption spectra. In order to overcome drawbacks due to the large number of atoms involved, for **2** and **1**, the study focussed first on computationally more affordable model dyes (hereafter dye **1a** and dye **2a**, see Scheme 2) derived from the same chromogenic system, substituting the aliphatic chains bearing functional bioconjugable groups with simple ethyl groups. Such simplification is made possible by the negligible contributions of non-aromatic side chains on the dye's frontier orbitals.

Please, insert here Scheme 2.

The study focussed on the effect of nitro groups as electron-withdrawing moieties conjugated to the aromatic system of a pentamethine cyanine on the UV-Vis absorption and photoemission spectra; a comparison was made with a non nitro-substituted pentamethine cyanine (dye **3**, Scheme 1). Afterwards, dye **2** is structurally fully characterized; the optimized geometry has been employed for the calculation of NMR parameters, which were used as an aid for NMR spectrum interpretation. Finally dye **2** is synthesised and its emission properties, together with those of dye **3**, are evaluated by means of UV-Vis spectroscopy and a quenching test for the RET pair dye **2**/dye **1** is presented.

2. Experimental

2.1 Computational Details

The work has been carried out within the Density Functional Theory (DFT) framework [17], using different functionals and basis sets. The calculation of vertical excitation energy (VEE) and the oscillator strength of low-lying singlet excited state were carried out at the equilibrium geometry using Time Dependent DFT (TD-DFT) [18,19].

According to the Franck-Condon principle, the maximum absorption peak (λ_{max}) in an UV-Vis spectrum corresponds to the vertical excitation. The simulation of the absorption spectra has been carried out using hybrid functional B3LYP [28] and TZVP basis set: as in all hybrid functionals, the exchange part is corrected by a prefixed amount of Hartree-Fock (nonlocal) exchange. This hybrid XC functional already proved to be a valuable choice for similar systems [23]. The optimization of the structure of the lower-energy excited state (S1) has been carried out in order to evaluate the maximum fluorescence emission of the dyes and the transition intensity.

We used structural minima for dye **2** to compute magnetic parameters, which proved to be a very useful tool to help assignment and interpretation of experimental NMR spectra. For the calculations of magnetic parameters the PBE1PBE hybrid density functional [29] has been used, which is known

to provide nuclear magnetic shieldings in excellent agreement with the experiment for a large number of organic molecules.

The chemical shielding tensor for nucleus N, σ^N, is given by the second-order response of the electronic energy E with respect to the external magnetic field $\boldsymbol{B}$ and the nuclei magnetic moment $\boldsymbol{m}_N$. To avoid problems related to the choice of the gauge origin, we worked within the GIAO (gauge invariant atomic orbital) framework [30,31]. Environmental effects on nuclear magnetic shieldings have been studied by means of the Polarizable Continuum Model (PCM) for the solvent [32].

All of the above calculations have been performed using the Gaussian 03 [33] and the TURBOMOLE software packages [34].

2.2 Instruments

^{1}H-NMR spectra were recorded on a Bruker AC-200 MHz or on a JEOL EX 400 instrument and referenced to tetramethylsilane. Mass spectra were recorded on a Thermo Finnigan Advantage Max Ion trap Spectrometer. UV-Vis absorption spectra were collected by a Perkin Elmer (Lambda 19) spectrometer. Steady state fluorescence spectra were recorded on a Horiba Jobin-Yvon spectrofluorimeter (Fluorolog 3, T-format spectrophotometer), and corrected for the spectral sensitivity of the photomultiplier (Hamamatsu R928). Absorption and emission spectra were recorded in spectroscopic grade methanol, at room temperature; in these conditions dyes are stable for weeks, if stored in the dark.

2.3 Synthesis

Starting materials were obtained from commercial suppliers (Sigma Aldrich and ACROS Organics). 2,3,3-Trimethyl-5-nitro-3H-indole was prepared through standard Fisher synthesis, starting from 3-methyl-2-butanone and 4-nitrophenylhydrazine according to literature methods (total yield on two steps: 59%, see SI for detailed references) [35]. 6-Iodohexyne [36] was prepared

following literature methods starting from 6-chlorohexyne (see SI for detailed synthesis and characterisation). 1-Amino-3-anilinopropan-1,3-diene or malonaldehyde dianilide was prepared through a standard condensation between aniline and tetramethoxy propane [37]. Dye **3** was prepared from 1-ethyl-2,3,3-trimethyl-3H-indolium iodide and malonaldehyde dianilide following a modification of literature methods [38, 39] (see S.I. for details and characterization).

2.3.1 *N-(Hex-5-ynyl)-2,3,3-trimethyl-5-nitro-3H-indolium iodide* **(2b).**

2,3,3-Trimethyl-5-nitro-3H-indole (4 mmol) and 6-iodohexyne (5,24 mmol) were dissolved in tetramethylene sulfone (9 ml) and refluxed for 13h at 130°C. The mixture was cooled down and diluted in diethyl ether (1000 ml). The red solid was filtered off and washed with diethyl ether until a powder was obtained. Yield: 49.1%

^{1}H NMR (DMSO-d_6): δ (ppm) 1.38 (s, 6H, 2CH_3), 1.62 (q, 2H, Hγ), 1.90 (m, 2H, H_δ), 2.37 (s, 3H, N^+=C-CH_3), 2.27 (m, 2H, H_β), 2.86 (d, 1H, ≡CH), 4.51 (t, 2H, H_α), 7.01 (d, 1H, H_7), 7.85 (dd, 1H, H_4), 8.33 (d, 1H, H_6).

MS-ESI (*m*/*z*) calcd 412, found 285 (M – Iodide); UV-Vis (methanol): λ_{max} = 403 nm

Anal. Calcd. for C17H21IN2O2 C, 49.53; H, 5.13; N, 6.79. Found: C, 49.7; H, 5.3; N, 6.9 %.

2.3.2 *6-(2,3,3-Trimethyl-5-nitro-3H-indolium-1-yl)hexanoate* **(2c)**

2,3,3-Trimethyl-5-nitro-3H-indole (4 mmol) and 6-iodohexanoic acid (14 mmol) were dissolved in tetramethylene sulfone (15 ml) and refluxed for 15h at 130°C. The mixture was cooled down and diluted in diethyl ether (1000 ml). The brown solid was filtered and washed with diethyl ether until free powder was obtained. Yield: 68.5%

^{1}H NMR (DMSO-d_6): δ (ppm) 1.28 (s, 6H, 2 CH_3), 1.47 (m, 2H, H_γ), 1.56 (s, 3H, N^+=C-CH_3), 1.62 (m, 2H, 2H, H_δ), 1.89 (m, 2H, H_β), 2.34 (t, 2H, H_ε), 4.35 (t, 2H, H_α), 7.84 (d, 1H, H_7), 8.11 (dd, 1H, H_4), 8.51 (d, 1H, H_6).

MS-ESI (*m*/*z*) calcd 318, found 319 (M + H); UV-Vis (methanol): λ_{max} = 415 nm

Anal. Calcd. for C17H22N2O4 C, 64.13; H, 6.97; N, 8.80. Found: C, 64.5; H, 7.1; N, 8.9 %.

2.3.3. *1,1,2-Trimethyl-1H-benzo[e]indole-7-sulfonate potassium salt* **(1b)**

Step 1: (6-Hydrazinonaphtalene-1-sulfonic acid): A suspension of 6-amino-1-naphthalensulfonic acid (0.086 mol) in 75 ml of 50% hydrochloric acid was stirred and maintained at 0-5°C. A solution of sodium nitrite (0.086g in 40 ml of water) was added dropwise. The rate of the addition was controlled to keep the temperature above 5°C. Cooling was continued while a solution of stannous chloride (60 g in 64 ml of concentrated HCl) was added dropwise to the stirred mixture at a rate to keep the temperature at or below 5 °C. After the addition of stannous chloride the stirring was continued for 1 h. The reaction was driven in dark and ice (80 g) was added to keep the mixture fluid. The mixture was stirred for 30 min. The precipitated product was filtered and washed with brine. The product was crystallized with the minimum amount of water necessary, then filtered and dried. The final product is a pink powder. Yield: 61.4%

^{1}H NMR (DMSO-d_6): δ (ppm) 7.16 (d, 1H, H_7), 7.24 (s, 1H, H_5), 7.38 (t, 1H, H_3), 7.67 (d, 1H, H_4), 7.82 (d, 1H, H_2), 8.74 (d, 1H, H_8). MS-ESI (*m*/*z*) calcd 238, found 237 (M – H); UV-Vis (methanol): λ_{max}= 280 nm (333 nm).

Step 2: (*1,1,2-Trimethyl-1H-benzo[e]indole-7-sulfonate potassium salt)*

A mixture containing the hydrazine from the previous preparation (0.042 mol), methyl isopropyl ketone (13.4 ml, 0.125 mol) and acetic acid glacial (25 ml) was refluxed at 135 °C for 3 h. The mixture was then cooled and n-hexane was added three times. After every addition the mixture was evaporated on a rotary evaporator under vacuum. The obtained product was a dark coloured gum. It was dissolved in methanol and added dropwise to diethyl ether (250 ml). The precipitated product was filtered and washed with diethyl ether until free powder was obtained. The product was then converted to the corresponding potassium salt. The solid was dissolved in methanol, then a solution of potassium hydroxide in 2-propanol was added. The solid was then filtered off and dried. The final product is a red-purple powder. Yield: 91.9 %

^{1}H NMR (DMSO-d_6): δ (ppm) 1.49 (s, 6H, 2 CH_3), 2.36 (s, 3H, N^+=C-CH_3), 7.58 (t, 1H, H_5), 7.73 (d, 1H, H_9), 8.03 (d, 1H, H_4), 8.12 (d, 1H, H_6), 9.00 (d, 1H, H_8). MS-ESI (*m/z*) calcd 327, found 288 (M – K). UV-Vis (methanol): λ_{max}= 280 nm (333 nm).

Anal. Calcd. for C15H14KNO3S C, 55.02; H, 4.31; N, 4.28; S, 9.79. Found: C, 55.2; H, 4.5; N, 4.4; S, 9.6%.

2.3.4. *3-(5-Carboxypentyl)-1,1,2-trimethyl-1H-benzo[e]indolium-6-sulfonate* **(1c)**

1,1,2-Trimethyl-1H-benzo[e]indole-7-sulfonate potassium salt (**1b**) (3.21 mmol) and 6-bromohexanoic acid (4.55 mmol) in tetramethylene sulfone (13 ml) were heated at 120°C for 12 h in an argon atmosphere. After that the mixture was cooled and the reaction mixture was diluted with toluene. The solid was filtered off, washed with toluene and dried. Yield: 92.3%

^{1}H-NMR (400 MHz, DMSO-d_6): δ (ppm) 1.48 (m, 2H, H_γ), 1.58 (m, 2H, H_δ), 1.75 (s, 6H, 2CH_3), 1.91 (m, 2H, H_β), 2.23 (t, 2H, H_ε), 2.95 (s, 3H, N^+=C-CH_3), 4.60 (t, 2H, H_α), 7.71 (t, 1H, H_5), 8.14 (d, 1H, H_9), 8.17 (d, 1H, H_6), 8.34 (d, 1H, H_4), 9.21 (d, 1H, H_8).

MS/ESI (*m/z*) calcd 403, found 404 $[M+H]^+$.

Anal. Calcd. for C21H25NO5S C,62.51; H, 6.25; N, 3.47; S, 7.95. Found: C, 62.7; H, 6.4; N, 3.3; S, 7.7%.

2.3.5 Dye 2

Step 1: hemicyanine

Malonaldehyde dianil hydrochloride (2.00 mmol), N-(hex-5-ynyl)-2,3,3-trimethyl-5-nitro-3H-indolium iodide **(2b)** (1.75 mmol), acetyl chloride (5 ml) and acetic anhydride (10 ml) were mixed and refluxed at 135°C. The evolution of the reaction was followed by the changes in UV-vis spectrum of the solution. After one hour the dark green mixture was cooled down and diluted with diethyl ether. The brown solid was filtered off and dried under vacuum. Yield: 59.4%.

UV-Vis (methanol): λ_{max} = 496 nm

Step 2: unsymmetrical cyanine (dye **2**)

Hemicyanine (1.04 mmol), 6-(2,3,3-trimethyl-5-nitro-3H-indolium-1-yl)hexanoate **(2c)** (1.51 mmol) and potassium acetate (1.66 mmol) in acetic anhydride (10 ml) were heated to reflux at 135°C for 1 h. The solution was cooled down and diluted with diethyl ether; the precipitate was filtered off and dried under vacuum. The crude product was purified by flash chromatography (Silica gel, dichloromethane/methanol 90:10 → dichloromethane/methanol 40:60) and MPLC (RP-C18, dioxane/acetonitrile 80/20) in order to separate the desired product from the symmetrical cyanine dyes formed in small quantities (ca. 5%). Yield: 47.2 %.

^{1}H NMR: (DMSO-d_6): δ (ppm) 1.61 (t, 2H, $H_{\delta'}$), 1.67 (m, 2H, $H_{\gamma'}$), 1.75 (s, 12H, -CH_3), 1.86 (m, 4H, H_β, H_γ), 1.92 (s, 1H, -C≡CH), 2.30 (m, 2H, H_δ), 2.6 (t, 2H, H_ε), 3.75 (t, 4H, H_α, $H_{\alpha'}$), 6.40 (m, 1H, H_A), 6.47 (m, 2H, H_C), 7.60 (d, 2H, H_7, $H_{7'}$), 8.40 (m, 2H, H_B), 8.50 (d, 2H, H_4, $H_{4'}$), 8.60 (d, 2H, H_6, $H_{6'}$); MS-ESI (*m*/*z*) calcd 766, found 639 (M – I); UV-Vis (methanol): λ_{max} = 663 nm (ε=250000 mol L cm^{-1})

Anal. Calcd. for C37H43IN4O6 C, 57.96; H, 5.65; I, 16.55; N, 7.31. Found: C, 58.2; H, 5.8; N, 7.0 %.

2.3.6 Dye 1

3-(5-Carboxypentyl)-1,1,2-trimethyl-1H-benzo[e]indolium-6-sulfonate (**1c**) (7.43 mmol), anhydrous potassium acetate (9.14 mmol) and N,N'-diphenylformamidine (3.7 mmol) were dissolved in acetic anhydride (40 ml) and stirred at 135°C for 2 hours. The reaction mixture was cooled down to room temperature, then it was diluted with diethyl ether. The formed precipitate was filtered and dried in vacuum overnight. The product was purified by MPLC (RP-C18, dichloromethane/methanol 90/10 → dichloromethane/methanol 40/60). Yield 65%

^{1}H NMR (DMSO-d_6): δ (ppm) 1.44 (m, 4H, H_γ), 1.56 (m, 4H, H_δ), 1.68 (s, 12H, CH_3), 1.94 (m, 4H, H_β), 2.26 (t, 4H, H_ε), 4.58 (t, 4H, H_α), 6.53 (d, 2H, H_B), 7.71 (t, 2H, H_5), 8.14 (d, 2H, H_9), 8.17 ($d_{[wd]}$, 2H, H_6), 8.35 (m, 3H, H_4+H_A), 9.21 (d, 2H, H_8); MS-ESI (*m*/*z*) calcd 855, found 815 (M – K)

Absorption (water): λ_{max}= 584 nm; ε = 160000 mol L cm^{-1}. Emission: λ_{max} = 592 nm.

Anal. Calcd. for C43H47KN2O10S2 C, 60.40; H, 5.54; N, 3.28; S, 7.50. Found: C, 60.8; H, 5.8; N, 3.5; S, 7.3%.

3. Results and Discussion

3.1 Computational Characterization

The calculation of the main absorption and emission wavelength has been carried out for trimethine-cyanine and the pentamethine-cyanine dyes using model systems in which the functionalized chains on the quaternary nitrogens have been substituted by ethyl moieties (**1a** and **2a**, see Scheme 2). As dye **3** already presents only ethyl groups on quaternary nitrogens, the structure has not been modified. This choice was based on the hypothesis of negligible contributions to the main electronic transitions from the aliphatic side chains and has been afterwards verified by molecular orbital analysis (*vide infra*).

In Table 1 the vertical excitation energies and the wavelengths corresponding to the transition that dominates the visible absorption and emission spectra are collected. Experimental values for excitation energies and the related λ_{max}abs, λ_{max}em are also reported.

Please, insert here Table 1

For all dyes the main transition is associated with the lowest-energy excited state, corresponding to a $\pi \rightarrow \pi^*$ HOMO – LUMO transition. Minor contributions to the absorption spectra are given by transitions involving indole localized orbitals. Such transitions present much smaller oscillator strengths, which allow us to focus our attention on the evaluation of the emission spectra to the first excited state only.

It has been shown [23] that TDDFT calculations usually overestimate the excitation energies of the $\pi \rightarrow \pi^*$ transition for cyanine dyes, but the errors are mostly systematic and can be corrected using appropriate linear scaling approaches. The remaining difference with respect to the experiment comes from the effects of the surrounding media and from the limitation of the exchange-

correlation functional. In this case, the average difference between calculated and experimental results is equal to 0.5 ± 0.03 eV. However, with these factors constant and due to the computational method, the comparison between optical properties of different dyes is made possible by the reliability of the trends of the computed data.

After relaxation of the excited state geometry, the HOMO-LUMO energy gap reduces by 0.08 eV for **2a**, 0.13 eV for **3** and 0.10 eV for **1a** , which correspond to Stokes shift of 19 nm, 28 nm and 23 nm respectively. These computed values agree well with the experimental values of 16.5 nm for **1** and 20 nm and 21 nm for **3** and **2**, respectively.

The presence of the electron withdrawing group on the aromatic system stabilizes the excited state of 0.05 eV, which is in good agreement with the experimental value (0.06 eV). This corresponds to a bathochromic shift of 11 nm (17 nm by experiment) in the absorption maximum of **2a** with respect to **3**. The effect of the nitro substituent on the photoemission spectra is less nicely reproduced, providing a stabilization of the excited state of 0.02 eV, versus an experimental value comparable to the absorption one (0.05 eV).

In order to estimate the energy transfer intensity, the calculation of donor emission and acceptor absorption spectra profile would be necessary. This can be done through an in-depth analysis of the vibrational states involved in the transitions [40]: however this computationally demanding procedure is beyond the scope of this paper. Quantitatively, the bathochromic shift in absorption and emission due to the nitro substituents allows to be more selective (in comparison to the use of non-nitrosubstitued cyanine, i.e. **3**) when exciting the donor/acceptor pair; in the same time a good overlap of the emission and absorption bands is maintained. The calculated optical properties of the **2a** suggests that **2** is a better candidate as a RET acceptor for the fluorescent dye **1**.

A deeper investigation on the structure and properties of compound **2** is presented. The most important geometrical parameters for the optimized ground and first excited states of dye **2** are collected in Table 2. A complete structural analysis of both states can be found in the supporting

materials. Since the molecule is symmetric, from the chromogen point of view, only the non-redundant geometrical parameters are reported.

Please, insert here Table 2

The molecule is mostly planar in both states, with the exception of a small angle between the plane of the indole ring and the polymethine chain. However, this angle is reduced from 2.6° to 1.7° going from the ground to the optimized excited state. Both relaxed structures show the characteristic feature of polymethine dyes with equal bond lengths in the polymethine chain, as a result of a highly delocalized electron density. The geometry relaxations are quite small and most of them correspond to the elongation of the CN and CC bonds, with the exception of the C3-C4 and the C11-N12 bonds.

The electron density of the frontier orbitals involved in the UV-Visible spectra are sketched in Figure 1.

Please, insert here Figure 1

The electron density is highly delocalized for both HOMO and LUMO, involving the polymethine chain and the indole rings, while the alkyl chains have negligible contribution to the frontier orbitals. The electron density is localized only on α and β positions of the aliphatic chain, thus validating our hypothesis on the possibility to substitute the linker arms with ethyl moieties when evaluating optical properties. In the LUMO, with respect to the HOMO, the electron density is localized also on the nitro substituents, explaining the stabilizing effect of the electron-withdrawing moiety on the excited state.

A magnetic parameter calculation has been performed on the equilibrium geometry of the ground state to evaluate the quality of the structure: the calculated proton chemical shift are reported in Table 3.

Please, insert here Table 3

Chemical shifts have been calculated as described above; the calculation of ^{1}H-NMR parameters have been carried out both in vacuum and in DMSO to mimic the experimental conditions [41]. A linear regression analysis has been performed on the calculated vs experimental results (Table 3): the agreement between experimental and computational data is very good and the solvent effect is shown by the better correlation between experimental and calculated data in DMSO than *in vacuo*. This agreement allowed us to use computational chemical shifts for the assignment of the signals in NMR spectrum.

3.2 Synthesis

Cyanine dyes were synthesized using modifications of methods previously described [38]. General scheme for the synthesis is reported in Scheme 3 (unsymmetrical dye **2**) and Scheme 4 (symmetrical dye **1**). Key intermediates for the syntheses of unsymmetrical and symmetrical cyanine dyes are the indolium salts **2b**, **2c** and **1c**. They were prepared in good to excellent yields starting from the related 2,2,3-trimethyl-1H-indole by quaternarization with a ω-functionalized long chain alkyl iodide (or bromide) in sulfolane at 135°C. Since 1,1,2-trimethyl-1H-benzo[e]indole-7-sulfonate potassium salt **1b** is not commercially available, 6-aminonaphthalene-1-sulfonic acid was first converted into the hydrazine hydrochloride, which was then subjected to Fischer indole condensation with methylbutanone.

Fluorophores and quenchers employed in PCR analysis need to be covalently bound to oligonucleotides by an appropriate spacer arm. Both the functional group used for the covalent bond

and the length of the spacer chain may influence the PCR response [42]. A new class of cyanine dyes have been developed, carrying a terminal alkyne functionality exploitable for direct linkage to halogen modified nucleotides [43].

The symmetrical trimethine cyanine dye **1** was prepared with the commonly used reaction mixture of N,N'-diphenylformamidine in acetic anhydride. Unsymmetrical pentamethine cyanine dye **2** was prepared by first reacting the alkynyl indolium salt with malonaldehyde dianilide in a mixture of acetic anhydride and potassium acetate. The crude dyes were purified by column chromatography (using both silica gel flash chromatography and RP-18 MPLC, see Experimental section for further details). Both intermediates and dyes were characterized by ^{1}H-NMR, Mass Spectrometry, UV-Vis and Fluorescence Spectroscopy.

Please, insert here Scheme 3 and Scheme 4

3.3 Spectroscopic Results

Dye **2** and dye **3** UV-Vis absorption and photoemission properties have been evaluated with regard to the possibility of employing them as acceptors with the donor **1** in a RET pair. UV-Vis absorption and emission spectra have been recorded in a range of concentrations in which quenching phenomena or inner filter effect do not occur. As shown in Figure 2, compound **2** and **3** display absorption bands similar in shape, but a different maxima absorption wavelength. The presence of nitro substituents influences the absorption maximum bringing about a bathochromic shift of 18 nm. The short wavelength shoulder present in the absorption spectra (that became bathochromic in emission spectra) of both dyes is typical of cyanines and related polymethine dyes. The assignment of the nature of these two components is given according to different interpretative models; the most recognized model for the interpretation of the cyanine dyes spectral profile correlates the main band to the (0,0) transition while the hypsochromic (or bathochromic) shoulders of the absorption (or emission) spectra are related to the vibrational modes of the excited and

ground states, respectively. Each shoulder is not determined by a unique vibrational normal mode, but by a collection of singly-excited vibrations [24].

Molar extinction coefficients (ε) have been calculated from the slope of a Lambert-Beer plot. Coefficients at the wavelength maxima are consistent for the two dyes, each showing a value around 250000 $M^{-1}cm^{-1}$ in methanol.

Please, insert here Figure 2

In Figure 2 absorption spectra of **3** (curve c) and **2** (curve d) are displayed with absorption and emission spectra of dye **1** (curves a and b respectively). It can be noticed that both the absorption band of **2** and that of **3** have a good overlap with the emission band of the donor **1**. Nevertheless, by comparing absorption spectra of the three dyes, we can observe that the absorption at the wavelength chosen for the excitation of the donor in RET/quenching experiments (i.e. 548 nm) is two fold higher for **3** with respect to compound **2** (Figure 2, in-set).

As a consequence, fluorescence intensity of **2** excited at 548 nm is lower than 40% of **3** emission (excited at the same wavelength), as shown in Figure 3; thus, the interference of acceptor fluorescence during the performance of a FRET experiment is minimal when **2** is used. We can therefore expect that **2** can act as a better acceptor dye, relative to the standard **3**, when used with **1** in a RET pair.

Furthermore, as expected, the emission spectra show a bathochromic shift of 20 nm going from 660 nm for **3** to 680 nm for **2**.

Please, insert here Figure 3

A RET/quenching test has been simulated experimentally without interacting species, by mixing donor and acceptor solutions at different donor/acceptor ratios. In Figure 4 the results of quenching tests at different donor **1**/acceptor **2** ratios are shown.

Please, insert here Figure 4

The donor concentration is set to $1 \cdot 10^{-7}$ M. Curve (a) shows the emission intensity of **1** in sodium borate buffer alone. Curves from (b) to (e) indicate the emission intensity recorded for solutions with increasing amounts of **2**. The donor **1**/acceptor **2** ratios investigated are 1:1 (curve b), 1:5 (curve c), 1:8 (curve d) and 1:10 (curve e). Photoemission intensity of **1** decreases along with the increasing concentration of **2**, without any significant increase in the intensity of the component that arise at 670 nm, that is due to the emission of the acceptor. Only part of the energy transferred by the donor to the acceptor is released in a radiative form; this may also be due to a self-quenching phenomena occurring for compound **2** concentrations higher than 1:5.

FRET efficiency (E%) was determined according to the equation

$$E\% = \left(1 - \frac{F_{DA}}{F_A}\right) \cdot 100$$

Where F_{DA} is the fluorescence intensity of the solution containing both the donor and the acceptor and F_A is the fluorescence intensity of the donor alone [44].

At the standard Real Time PCR and FRET experiment working ratio (1:1), the quenching efficiency is 51%, which suggests a profitable use of dye **2** for such applications.

4. Conclusions

A new nitro pentamethine indocyanine dye (compound **2**) has been designed, with the assistance of DFT calculations, and then synthesised with a view to use as a fluorescence quencher in a donor/acceptor pair for Real Time PCR analysis. This molecule has been functionalized with one

nitro group on each indole ring and brings two functionalized alkyl arms (directly linked to the nitrogen of the indole ring) for the bioconjugation with nucleotides. One of the spacer arms is functionalized with an alkyne group, while the other with a carboxylic acid group.

Structural effects on optical properties have been studied by time-dependent density functional theory, using B3LYP hybrid XC functional. Optical properties of **2** have been compared to those of the parent dye **3**, which is lacking nitro groups. Maximum intensity wavelengths of the absorption and photoemission spectra for the donor **1** and acceptors **2** and **3** have been carried out on model systems bearing ethyl moieties instead of the functional alkyl side chains. The analysis of the electron density of the frontier orbitals (involved in the transition dominating the spectra) proves that only the carbon atoms in α and β positions in the alkyl chains in respect to the aromatic system are involved in the $\pi \rightarrow \pi^*$ transition, thus validating such an approximation.

The systematic over estimation of the excitation energies provided by TD-DFT calculations is by-passed by the comparison of energy differences between the nitro-substituted dye and a reference dye.

The spectroscopic characterization proves that **2** is a good RET acceptor for **1** as the maximum absorption wavelength is bathochromically shifted by 20 nm, yet providing a good overlap with the emission band of the donor. Moreover, it was found that **2** bears a partial quenching capability.

As a preliminary test of the quenching efficiency of **2**, we measured the emission intensity of a solution containing the fluorescent dye **1** and the quencher **2**: for a concentration ratio of 1:1 the quenching efficiency for **2** is 51%.

5. Acknowledgements

The authors acknowledge financial support by Regione Piemonte (Progetto NANOMAT, Docup 2000-2006, Linea 2.4a; Ricerca Scientifica Applicata 2004, project codes D14 and D67).

ClB and GV thank Compagnia di San Paolo (Torino, Italy) and Fondazione della Cassa di Risparmio di Torino (Italy) for continuous supply of laboratory equipment.

Authors are also grateful to Centro ReTe – Università di Torino for computational support.

6. References

1. Higuchi R, Dollinger G, Walsh PS, Griffith R. Simultaneous amplification and detection of specific DNA sequences. Biotechnology 1992; 10:413–417.

2. Higuchi R., Fockler C, Dollinger G, Watson R. Kinetic PCR: Real time monitoring of DNA amplification reactions. Biotechnology 1993; 11:1026–1030.

3. Gambini MR, Atwood JG, Young EF, Lakatos EJ, Cerrone AL. Instrument for monitoring polymerase chain reaction of DNA, US2007154939.

4. Knobel R. Analytical method and instrument, WO2007071349.

5. Andrews, D.L. Mechanistic principles and applications of resonance energy transfer, Can.J. Chem 86 (2008), 855-870.

6. Bertolino CA, Caputo G, Barolo C, Viscardi G, Coluccia S. Novel heptamethine cyanine dyes with large Stokes' shift for biological applications in the near infrared. Journal of Fluorescence 2006; 16:221-225. (b) Hilderbrand SA, Kelly KA, Weissleder R, Tung CH. Monofunctional near-infrared fluorochromes for imaging applications. Bioconjugate Chemistry 16 (2005), 1275-1281. (c) Patonay G, Salon J, Sowell J, Strekowski L Molecules, 9 (2004), 40-49.

7. Iqbal A, Wang L, Thompson KC, Lilley DMJ, Norman DG. The structure of Cyanine5 terminally attached to double-stranded DNA: implications for FRET studies. Biochemistry 2008; 47:7857-7862.

8. Bouteiller C, Clavé G, Bernardin A, Chipon B, Massoneau M, Renard P-Y, Romieu A. Bioconjugate chemistry 2007 ; 18 :1303-1317.

9. Haugland R, Cheung C-Y, Yue S. Cyanine compounds and their application as quenching compounds. U.S. Pat. Appl. Publ.: US 2005191643.

10. Miyako T, Moriwaki K. Composition for optical film comprising a near-infrared absorbing dye and a quencher. Eur. Pat. Appl.: EP 1496375.

11. Fabian, J, Hartmann, H, Light Absorption of Organic Colorants, (1980) Springer-Verlag, Berlin Heidelberg, New York.

12. Peng XX, Xinshe D, Daniel R, Little GM, Chen J, Volcheck WM, Prescott, C. Near IR-absorbing nonfluorescent cyanine dyes for probe labeling. PCT Int. Application: WO 2007005222.

13. Diwu Z, Zhang J, Tang, Y. Cyanine dyes and their applications as luminescence quenching compounds. US Patent Application: US 2006/0223076.

14. Lee LG, Graham RJ, Mullah KB, Haxo FT. Nitro-substituted non-fluorescent asymmetric cyanine dye compounds. US Patent 7166715.

15. Della Ciana L, Grignani A, Cassullo M, Caputo G, Sulfobenz(e)indocyanine fluorescent dyes and their use. PCT Int. Appl. 1997; WO 9713810.

16. Marras SAE, Kramer FR, Tyagi S. Efficiencies of fuorescence resonance energy transfer and contact-mediated quenching in oligonucleotide probes Nucleic Acid Research 2002; 30:e122.

17. Dreizler R, Gross E, Density Functional Theory, Plenum Press, New York, 1995.

18. Bauernshmitt R, Ahlrichs R Treatment of electronic excitations within the adiabatic approximation of time dependent density functional theory Chemical Physics Letters 1996; 256:454-464.

19. Stratmann RE, Scuseria GE, Frisch MJ. An efficient implementation of time-dependent density-functional theory for the calculation of excitation energies of large molecules. Journal Chemical Physics 1998; 109:8218-8224.

20. Improta R, Santoro F. A theoretical study on the factors influencing cyanine photoisomerization: the case of thiacyanine in gas phase and in methanol Journal of Chemical Theory and Computation 2005; 1:215-229.

21. Jacquemin D, Perpète EA, Scalmani G, Frisch MJ, Kobayashi R, Adamo C. Assessment of the efficiency of long-range corrected functionals for some properties of large compounds. Journal of Chemical Physics 2007; 126:144105(1)-144105(12).

22. Schreiber M, Buß V, Fülscher MP. The electronic spectra of symmetric cyanine dyes: a CASPT2 study. Physical Chemistry Chemical Physics 2001, 3:3906-3912.

23. Champagne B, Guillaume M, Zutterman F TDDFT investigation of the optical properties of cyanine dyes Chemical Physics Letters 2006; 425:105-109.

24. Guillaume M, Liégois V, Champagne B, Zutterman F. Time-dependent density functional theory investigation of the absorption and emission spectra of a cyanine dye. Chemical Physics Letters 2007; 446:165-169.

25. Vladimirova KG, Freidzon Aya, Bagatur'yants AA, Zakharova GV, Chibisov AK, Alfimov MV. Modeling the structure, absorption spectra, and cis-trans isomerization of thiacarbocyanine dyes. Energy Chemistry 2008; 42:317-324.

26. Baraldi I, Brancolini G, Momicchioli F, Ponterini G, Vanossi D Solvent influence on absorption and fluorescence spectra of merocyanine dyes: a theoretical and experimental study. Chemical Physics 2003; 288:309-325.

27. Bertolino CA, Ferrari AM, Barolo C, Viscardi G, Caputo G, Coluccia S. Solvent effect on indocyanine dyes: a computational approach. Chemical Physics 2006; 330:52-59.

28. Becke AD. Density-functional thermochemistry. III. The role of exact exchange Journal Chemical Physics 1993; 98: 5648-5652.

29. Adamo C, Barone V. Toward reliable density functional methods without adjustable parameters: The PBE0 model. Journal of Chemical Physics 1999; 110:6158.

30. Wolinski K, Hilton JF, Pulay P. Efficient implementation of the gauge-independent atomic orbital method for NMR chemical shift calculations Journal of the American Chemical Society 1990; 112:8251-8260.

31. Keith TA, Bader RFW. Calculation of magnetic response properties using a continuous set of gauge transformations Chemical Physics Letters 1993; 210:233-231.

32. Miertus S, Scrocco E, Tomasi J. Electrostatic interaction of a solute with a continuum. A direct utilization of ab initio molecular potentials for the prevision of solvent effects. Chemical Physics 1981; 55:117.

33. Gaussian 03, Revision C.02, Frisch, M. J.; Trucks G W, Schlegel HB, Scuseria, GE, Robb MA, Cheeseman JR, Montgomery Jr.JA, Vreven T, Kudin KN, Burant JC, Millam JM, Iyengar SS, Tomasi J, Barone V, Mennucci B, Cossi M, Scalmani G, Rega N, Petersson GA, Nakatsuji H, Hada M, Ehara M, Toyota K, Fukuda R, Hasegawa J, Ishida M, Nakajima T, Honda Y, Kitao O, Nakai H, Klene M, Li X, Knox JE, Hratchian HP, Cross JB, Bakken V, Adamo C, Jaramillo J, Gomperts R, Stratmann RE, Yazyev O, Austin AJ, Cammi R, Pomelli C, Ochterski JW, Ayala PY, Morokuma K, Voth GA, Salvador P, Dannenberg J J, Zakrzewski VG, Dapprich S, Daniels AD, Strain MC, Farkas O, Malick DK, Rabuck AD, Raghavachari K, Foresman JB, Ortiz JV, Cui Q, Baboul AG, Clifford S, Cioslowski J, Stefanov BB, Liu G, Liashenko A, Piskorz P, Komaromi I, Martin RL, Fox DJ, Keith T, Al-Laham MA, Peng CY, Nanayakkara A, Challacombe M, Gill PMW, Johnson B, Chen W, Wong MW, Gonzalez C, and Pople JA, Gaussian. Inc. Wallingford CT, 2004.

34. TURBOMOLE, Program Package for ab initio Electronic Structure Calculations, University of Karlsruhe, Germany, ver 5.71.

35. (a) Shaw E, Woolley DW. The Synthesis of Nitro- and Aminoindoles Analogous to Serotonin Journal of the American Chemical Society 1953; 75:1877-81; (b) Murphy S, Yang X, Schuster GB. Cyanine Borate Salts That Form Penetrated Ion Pairs in Benzene Solution: Synthesis, Properties, and Structure Journal of Organic Chemistry 1995; 60: 2411-22.

36. Finkelstein H. Preparation of Organic Iodides from the Corresponding Bromides and Chlorides. Berichte der Deutschen Chemischen Gesellschaft 1910; 43:1528-32.

37. Jelinek CF, Kleinschmidt RF. Preparation of malonaldehyde dianils. 1951; US 2549097 19510417.

38. (a) Della Ciana L, Grignani A, Cassullo M, Caputo G. Sulfobenz(e)indocyanine fluorescent dyes and their use. PCT Int. Appl. 1997; WO 9713810; (b) Caputo G, Della Ciana L. New fluorescent cyanine labels containing a sulfonamido linker arm. Eur. Pat. Appl. 2001; EP 1065250; (c) Caputo G, Cyanine-type compounds having an alkynyl linker arm. PCT Int. Appl. 2005; WO 2005014723; (d) Caputo G, Della Ciana L, Improved process and method for the preparation of

asymmetric monofunctionalized indocyanine labelling reagents and obtained compounds, Patent Application EP1209205A1.

39. (a) Deichmeister MV, Levkoev II, Lifshits EB. Merocyanine dyes, derivatives of rhodanine. V. Some tetra- and hexamethinemerocyanines, derivatives of 3-ethylrhodanine. Zhurnal Obshchei Khimii. 1953; 23:1529-35; (b) Brooker LGS, Keyes GH, Sprague RH, VanDyke RH, VanLare E, VanZandt G, White FL, Cressman HWJ, Dent SG, Jr. Color and Constitution. Absorption of the merocyanines. Journal of the American Chemical Society 1951; 73:5332-50.

40. Borrelli R, Peluso A. Dynamics of radiationless transitions in large molecular systems: a Franck-Condon-based method accounting for displacements and rotations of all normal coordinates, Journal of Chemical Physics 2003; 119:8437-8448.

41. Benzi C, Crescenzi O, Pavone M, Barone V Reliable NMR chemical shifts for molecules of biological interest in condensed phases by methods rooted in the density functional theory, Magnetic Resonance in Chemistry 2004; 42:S57- 67.

42. Randolph JB, Waggoner AS. Stability, specificity and fluorescence brightness of multiply-labeled fluorescent DNA probes Nucleic Acids Research 1997; 25: 2923-2929.

43. Caputo G, Della Ciana L. Improved process and method for the preparation of asymetric monofunctionalized indocyanine labelling reagents and obtained compounds, Patent Application EP1209205A1.

44. Fung BKK, Stryer L. Surface density determination in membranes by fluorescence energy transfer Biochemistry 1978; 17:5241-5148.

Captions.

Table 1. Calculated and experimental S_0-S_1 energy gaps (in eV) and absorbance and emission wavelength (in nm) for the donor and the acceptor dyes.

Table 2. Main computed structural parameters for the ground and the first excited state of dye **2**. Labels for heavy atoms can be found in scheme 1.

Table 3. Experimental and computational chemical shift for dye **2**. Computational data are given both in vacuo and in DMSO.

Scheme 1. Dyes structures. Labels indicate heavy atoms.

Scheme 2. Model dyes for TD-DFT calculations.

Scheme 3. Synthetic route to dye **2**. a: preparation of intermediates; b: synthesis of the chromogen.

Scheme 4. Synthetic route to donor dye **1**. a: preparation of intermediates; b: synthesis of the chromogen.

Fig. 1 Schematic drawing of the HOMO (top) and the LUMO (bottom) orbitals of dye **2** *in vacuo.*

Fig. 2 Absorption (a) and Emission (b) profiles of donor dye **1** and absorption profiles of dye **3** (c) and dye **2**(d).

Fig. 3. Emission spectra of dye **3** (—) and dye **2** (---) at a concentration of $5 \cdot 10^{-7}$ M in methanol excited at 548 nm.

Fig.4 Quenching test: a) donor **1** at a concentration of $1 \cdot 10^{-7}$M; b) donor **1**/acceptor **2** 1:1; c) donor **1**/acceptor **2** 1:5; d) donor **1**/acceptor **2** 1:8; e) donor **1**/acceptor **2** 1:10 in sodium borate buffer, excitation at 548 nm.

Supporting Information

^{1}H-NMR spectra were recorded on a Bruker AC-200 MHz or on a JEOL EX 400 instrument and referenced to tetramethylsilane. Mass spectra were recorded on a Thermo Finnigan Advantage Max Ion trap Spectrometer. GC-MS (Gas Chromatography-Mass Spectrometry) analyses were performed on a Thermo Finnigan Trace MS-Plus equipped with an EI (Electronic Impact) ionization source and Ion Trap analyzer. UV-Vis absorption spectra were collected by a Perkin Elmer (Lambda 19) spectrometer. Steady state fluorescence spectra were recorded on a Horiba Jobin-Yvon spectrofluorimeter (Fluorolog 3, T-format spectrometer), and corrected for the spectral sensitivity of the photomultiplier (Hamamatsu R928). Absorption and emission spectra were recorded in spectroscopic grade methanol, at room temperature; in these conditions dyes are stable for weeks, if stored in the dark.

4-Nitrophenylidrazone

4-Nitrophenylidrazine (32 mmol) was dissolved in ethanol and mixed to 3-methyl-2-butanone (98 mmol). The mixture was heated at 120°C for 3h, under stirring. The obtained solution, dark red, was dried and redissolved in water (10 ml) and alkalinized to pH=8 with NaOH. The solution was extracted by ethyl acetate and the organic phase was dehydrate by sodium sulphate anhydrous. A brown oil was obtained. Yield: 74.6%.

^{1}H-NMR (DMSO-d_6) δ (ppm) 1.14 (s, 6H, CH_3), 1.87 (s, 3H, CH_3), 2.56 (s, 1H, CH), 7.04 (d, 2H, H_2 e H_6), 8.09 (d, 2H, H_3 e H_5). GC-MS (CH_2Cl_2)[M^+]: 221.

2,3,3-Trimethyl-5-nitro-3H-indole

4-Nitrophenylidrazone (24 mmol) was dissolved in hydrochloric acid 37% (70ml) and heated at reflux. After 3h, the brown mixture was cooled down to room temperature. The solution was alkalinized by NaOH and extracted with ethyl acetate. The crude product was dehydrate by sodium

sulphate anhydrous. The final product, a partially crystalline brown oil, was purified by flash chromatography using CH_2Cl_2 as eluent. Yield: 79.2%

^{1}H-NMR ($CDCl_3$): δ (ppm) 1.363 (s, 6H, -CH_3), 2.348 (s, 3H, N^+=C-CH_3), 7.583 (d, 1H, H_7), 8.145 (d, 1H, H_4), 8.221 (dd, 1H, H_6); MS-ESI (m/z) calcd 204, found 204 (M^+).

6-Iodo-1-hexyne

Sodium iodide (123.7 g, 0.83 mol) was dried overnight in oven at 150°C, then it was suspended in 300 ml of anhydrous acetone and vigorously stirred, then 25 ml of 6-chloro-1-hexyne (d 0.962 g/ml; 0.41 mol) were added dropwise. The reaction mixture was heated at 70°C and reacted at reflux for 24 hours. The mixture was then cooled at r.t. and the solvent was evaporated. The so obtained product was diluted in diethyl ether and filtered to separate formed NaCl. The yellowish liquid was extracted with Na_2SO_3 10%, $NaHCO_3$ 5% and deionised water. The combined organic layers were then dried with Na_2SO_4 at 4°C. After filtration, the solvent was evaporated and the product was obtained as a yellowish oil with a 100% yield. Rf=0.57 (SiO_2; Cyclohexane 100%)

^{1}H-NMR ($CDCl_3$): δ (ppm) 1.71 (m, 2H, $CH_2\gamma$), 1.94 (m, 3H, $CH_2\beta$ + ≡CH), 2.20 (td, 2H, $CH_2\delta$), 3.20 (t, 2H, $CH_2\alpha$). GC-MS EI $[M]^+$:208

1,2,3,3-Tetramethyl-3H-indolium iodide

2,3,3-Trimethyl indole (0.062 mol) and ethyl iodide (0.311 mol) were refluxed at 100°C for 1 hour. The reaction mixture was than cooled at r.t. and diluted with diethyl ether. The formed precipitate was collected, washed with diethyl ether and dried under vacuum overnight. Yield 89%.

^{1}H-NMR (DMSO-d_6) δ (ppm) 1.54 (s, 3H, -CH_3), 1.71 (s, 12H, -CH_3), 2.76 (s, 3H, N^+=C-CH_3), 4.48 (q, 2H, CH_2), 7.30 (t, 2H, H_2), 7.44 (m, 4H, H_3+H_4), 7.72 (d, 2H, H_1). MS-ESI (m/z) calcd 315.2, found 315 (M^+).

*Dye **3***

1,2,3,3-Tetramethyl-3H-indolium iodide (17.4 mmol), malonaldehyde dianil hydrochloride (8.67 mmol) and potassium acetate (21.1 mmol) were dissolved in 250 ml of acetic anhydride and stirred at 140°C for 2 hours. The reaction mixture was then diluted with diethyl ether; the precipitated product was filtered and dried under vacuum. The crude product was purified by flash chromatography (Silica gel, dichloromethane/methanol 90:10 → dichloromethane/methanol 40:60). Yield: 95%

^{1}H-NMR (DMSO-d_6) δ (ppm) 1.52 (s, 3H, -CH_3), 1.69 (s, 12H, -CH_3), 4.42 (q, 2H, CH_2), 6.28 (d, 2H, H_a), 6.57 (t, 1H, H_c), 7.26 (t, 2H, H_2), 7.41 (m, 4H, H_3+H_4), 7.63 (d, 2H, H_1), 8.34 (t, 2H, H_b). MS-ESI (m/z) calcd 411.6, found 411 (M^+); UV-Vis (methanol): λ_{max} = 640 nm (ε=250000 mol L cm^{-1})

Table S1. Geometrical parameters for the ground state of dye **2**. Labels for heavy atoms can be found in scheme 1.

Distances (Å)		Angles(degree)		Dihedral angles (degree)	
C1-C2	1.391	C1-C2-C3	124.1	C1-C2-C3-C4	-179.9
C2-C3	1.395	C2-C3-C4	126.1	C2-C3-C4-C5	-2.6
C3-C4	1.391	C3-C4-C5	128.3	C3-C4-C5-C6	-178.0
C4-C5	1.530	C5-C6-C7	130.5	C4-C5-C6-C7	179.8
C5-C6	1.511	C6-C7-C8	117.3	C5-C6-C7-C8	180.0
C6-C7	1.380	C7-C8-C9	122.8	C6-C7-C8-C9	0.0
C7-C8	1.394	C8-C9-C10	119.8	C7-C8-C9-C10	0.0
C8-C9	1.390	C9-C10-C11	117.3	C8-C9-C10-C11	0.0
C9-C10	1.391	C11-N12-C4	128.6	C9-C10-C11-N12	179.5
C10-C11	1.391	C4-C5-C13	111.6	C3-C4-C5-C14	-64.8
C11-N12	1.401	C4-C5-C14	111.9	C7-C8-N15-O16	-0.2
C5-C13	1.539	C7-C8-N15	118.4	C10-C11-N12-C19	0.5
C5-C14	1.539	C8-N15-O16	117.1	C11-N12-C19-C20	91.0
C8-N15	1.464	C8-N15-O17	117.4	N12-C19-C20-C21	180.0
N15-O16	1.218	O16-N15-O17	125.5	C19-C20-C21-C22	-180.0
N15-O17	1.218	C11-N12-C19	122.6	C20-C21-C22-C23	179.1
N12-C19	1.457	N12-C19-C20	112.9	C21-C22-C23-C24	0.8

C19-C20	1.527	C19-C20-C21	111.6	C1-C25-C26-C27	180.0
C20-C21	1.525	C20-C21-C22	112.2	C25-C26-C27-C28	-2.5
C21-C22	1.534	C21-C22-C23	112.4	C26-C27-C28-C29	-178.2
C22-C23	1.457	C22-C23-C24	178.7	C27-C28-C29-C30	179.7
C23-C24	1.207	C1-C25-C26	124.1	C28-C29-C30-C31	-179.7
C1-C25	1.392	C25-C26-C27	126.0	C29-C30-C31-C32	0.1
C25-C26	1.394	C26-C27-C28	128.5	C30-C31-C32-C33	-0.2
C26-C27	1.391	C27-C28-C29	101.2	C31-C32-C33-C34	-0.1
C27-C28	1.530	C28-C29-C30	130.5	C32-C33-C34-N35	-179.4
C28-C29	1.511	C29-C30-C31	117.3	C33-C34-N35-C27	-178.5
C29-C30	1.380	C30-C31-C32	122.8	C26-C27-C28-C36	64.7
C30-C31	1.394	C31-C32-C33	119.8	C29-C30-C31-N38	179.9
C31-C32	1.390	C32-C33-C34	117.3	C30-C31-N38-O39	0.2
C32-C33	1.391	C33-C34-N35	128.6	C33-C34-N35-C41	-1.0
C33-C34	1.391	C27-C28-C36	111.8	C34-N35-C41-C42	-89.4
C34-N35	1.401	C30-C31-N38	118.4	N35-C41-C42-C43	178.4
C28-C36	1.539	C31-N38-O39	117.1	C41-C42-C43-C44	178.9
C28-C37	1.539	C31-N38-O40	117.4	C42-C43-C44-C45	179.1
C31-N38	1.464	C34-N35-C41	125.5	C43-C44-C45-C46	177.0
N38-O39	1.220	N35-C41-C42	112.7	C44-C45-C46-O47	-4.7
N38-O40	1.218	C41-C42-C43	112.1	C44-C45-C46-O48	175.6
N35-C41	1.457	C42-C43-C44	112.1		
C41-C42	1.526	C43-C44-C45	112.8		
C42-C43	1.526	C44-C45-C46	112.1		
C43-C44	1.525	C45-C46-O47	125.3		
C44-C45	1.521	C45-C46-O48	111.5		
C45-C46	1.508	O47-C46-O48	123.2		
C46-O47	1.208				
C46-O48	1.343				

Table1

Table 1.

	Calculated ΔE (λ_{max})	Exp. ΔE (λ_{max})
Dye **1a**[(a)]		
absorbance	2.58 (481)	2.11 (586)
emission	2.48 (500)	2.06 (602)
Dye **3**		
absorbance	2.46 (503)	1,94 (640)
emission	2.33 (531)	1,88 (660)
Dye **2a**[(b)]		
absorbance	2.41 (514)	1.88 (658)
emission	2.31 (536)	1,83 (677)

(a) Experimental data are for Dye **1**.

(b) Experimental data are for Dye **2**.

Table 2. Main computed structural parameters

Table 2.

bond length (Å)			*bond angle (degree)*			*dihedral angle (degree)*		
	S_0	**S_1**		**S_0**	**S_1**		**S_0**	**S_1**
C1-C2	1.391	1.395	C1-C2-C3	124.1	124.5	C1-C2-C3-C4	-179.9	179.5
C2-C3	1.395	1.404	C2-C3-C4	126.1	126.4	C2-C3-C4-C5	-2.6	-1.7
C3-C4	1.391	1.386	C3-C4-C5	128.6	128.9	C3-C4-C5-C6	-178	-178.5
C4-C5	1.530	1.534	C4-C5-C6	101.2	101.1	C4-C5-C6-C7	-179.8	179.6
C5-C6	1.511	1.515	C5-C6-C7	130.5	130.2	C5-C6-C7-C8	180	180
C6-C7	1.380	1.376	C6-C7-C8	117.3	117.7	C6-C7-C8-C9	0	0
C7-C8	1.394	1.396	C7-C8-C9	122.8	122.5	C7-C8-C9-C10	0	0
C8-C9	1.390	1.397	C8-C9-C10	119.8	120.0	C8-C9-C10-C11	0	0
C9-C10	1.391	1.385	C9-C10-C11	117.3	117.7	C9-C10-C11-N12	179.5	-179.6
C10-C11	1.391	1.400	C10-C11-N12	128.6	128.9	C10-C11-N12-C4	-178.4	-179
C11-C6	1.395	1.406	C11-N12-C4	111.6	111.4	C7-C8-N15-O16	0.2	0.2
C11-N12	1.401	1.384	C7-C8-N15	118.4	118.6			
N12-C4	1.354	1.383	C8-N15-O16	117.1	117.3			
C5-C13	1.539	1.548	O17-N15-O16	125.5	125.1			
C5-C14	1.539	1.548						
C8-N15	1.464	1.475						
N15-O16	1.220	1.226						
N15-O7	1.221	1.225						

Table3

Table 3.

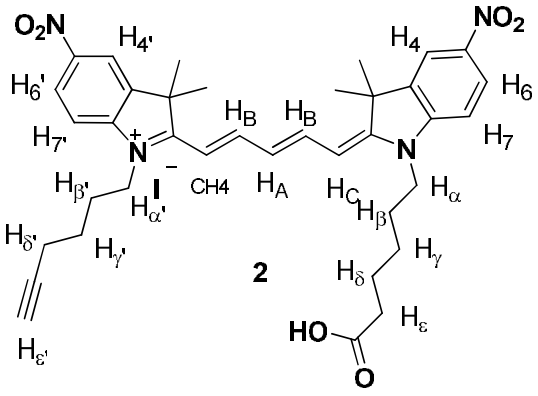

	Experimental	Calculated	
		in vacuo	in DMSO
H_6	8.6	8.99	9.09
H_4	8.5	8.80	8.96
H_B	8.4	8.03	8.09
OH	8.2	6.30	7.80
H_7	7.6	7.30	7.78
H_C	6.47	6.53	7.14
H_A	6.4	6.20	6.62
H_α	3.75	3.83	4.06
$H_{\alpha'}$	3.75	3.79	4.03
H_ε	2.6	2.40	2.57
H_δ	2.3	2.13	2.32
$H_{\varepsilon'}$	1.92	2.12	2.40
H_β	1.86	1.78	1.79
H_γ	1.86	1.65	1.75
CH_3	1.75	1.68	1.70
$H_{\delta'}$	1.61	1.69	1.58
$H_{\gamma'}$	1.67	1.34	1.48
slope		0.97	0.96
intercept		-0.05	0.11
R		0.9854	0.9957

Scheme_1

Scheme 1

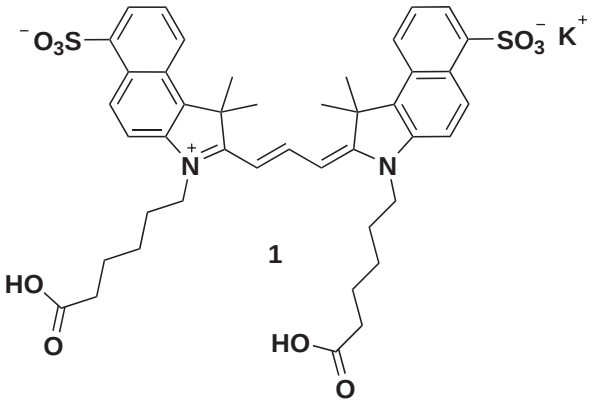

1

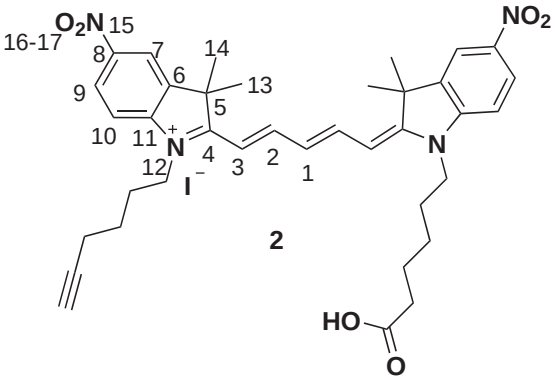

2

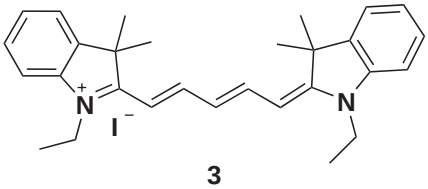

3

Scheme_2

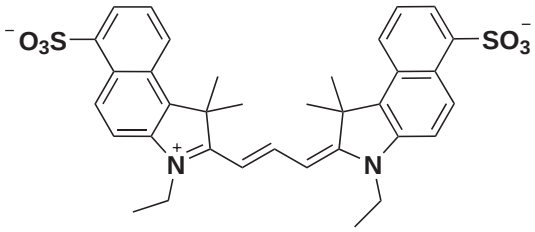

1a

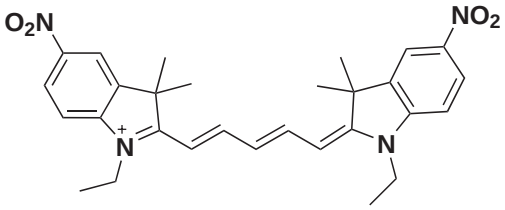

2a

Scheme_3

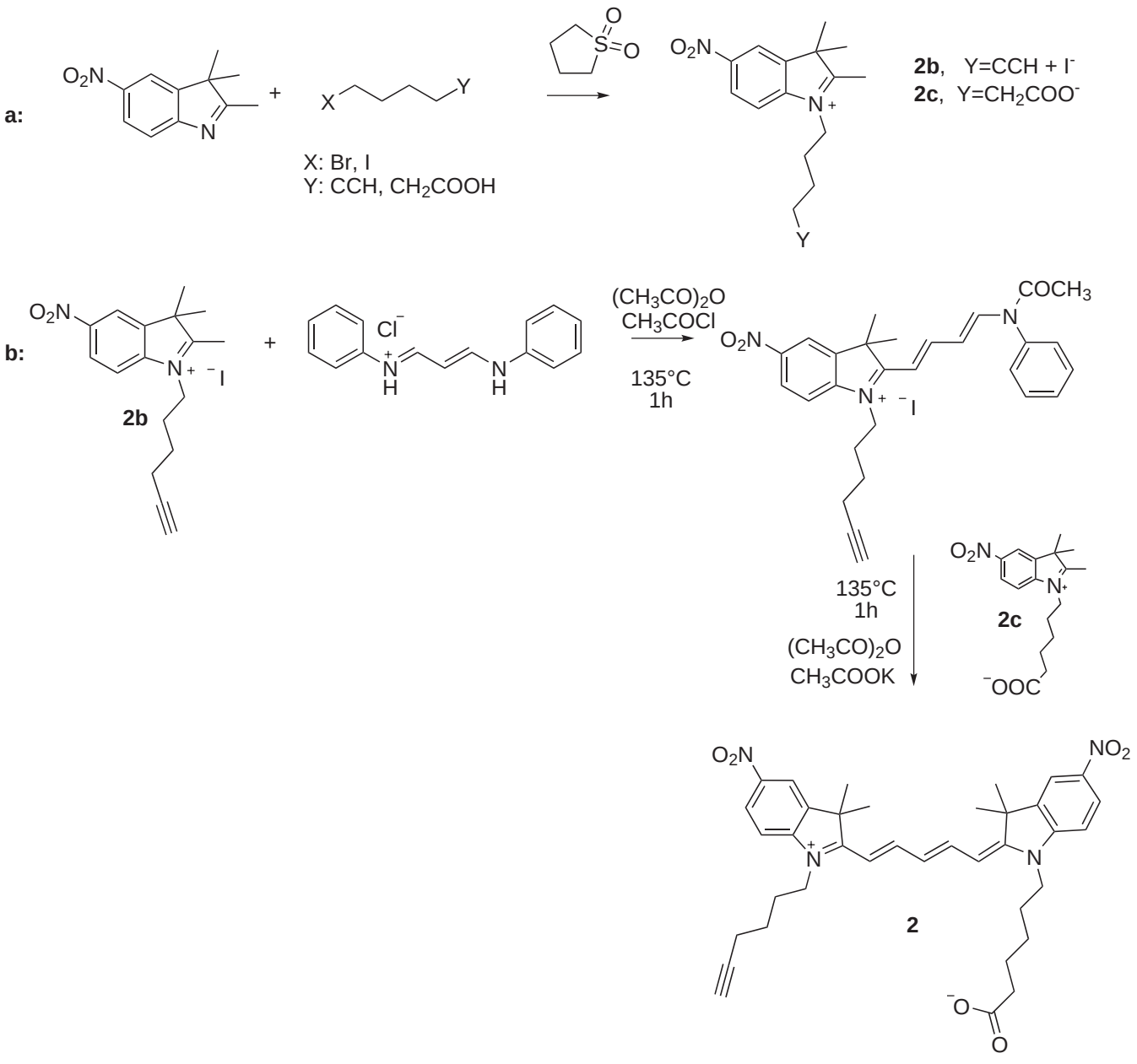
a:
X: Br, I
Y: CCH, CH2COOH
2b, Y=CCH + I-
2c, Y=CH2COO-
b:
2b
(CH3CO)2O
CH3COCl
135°C
1h
135°C
1h
(CH3CO)2O
CH3COOK
2c
2

Scheme_4

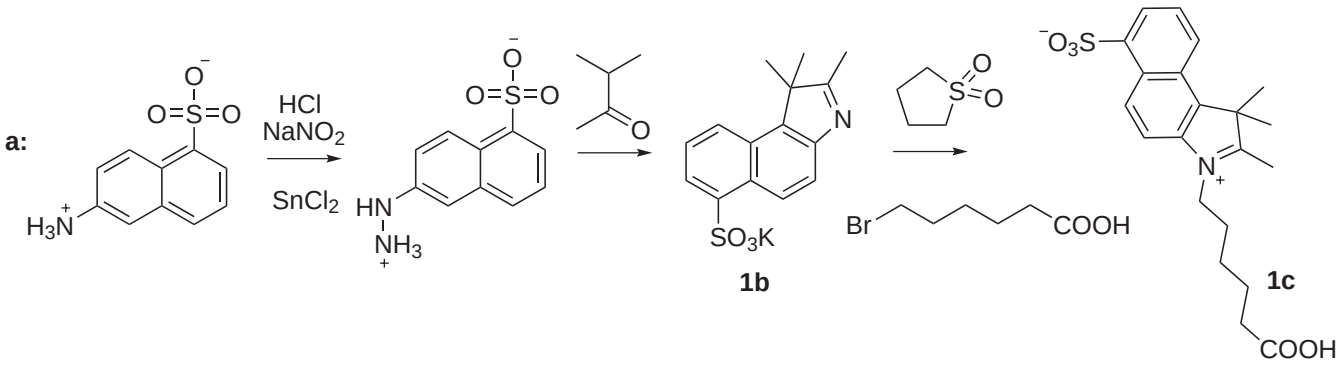
a:
HCl
NaNO2
SnCl2
1b
Br
COOH
1c
COOH

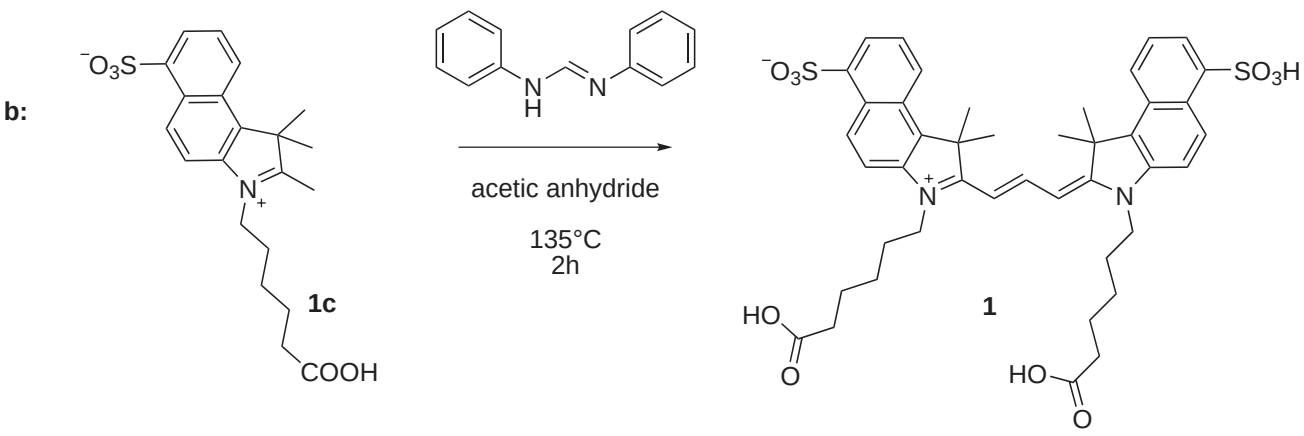
b:
1c
COOH
acetic anhydride
135°C
2h
1
HO
O
HO
O

Fig. 1 Schematic drawing of the HOMO (top) and the LUMO (bottom)

Figure 1.

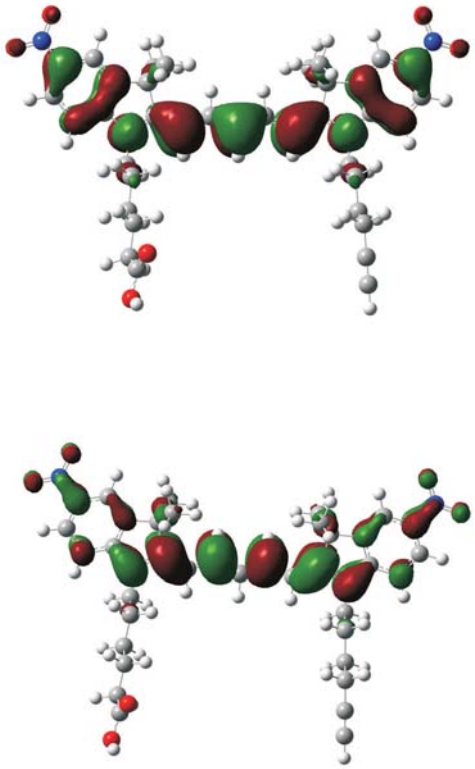

Fig. 2 Absorption (a) and Emission (b) profiles

Figure 2

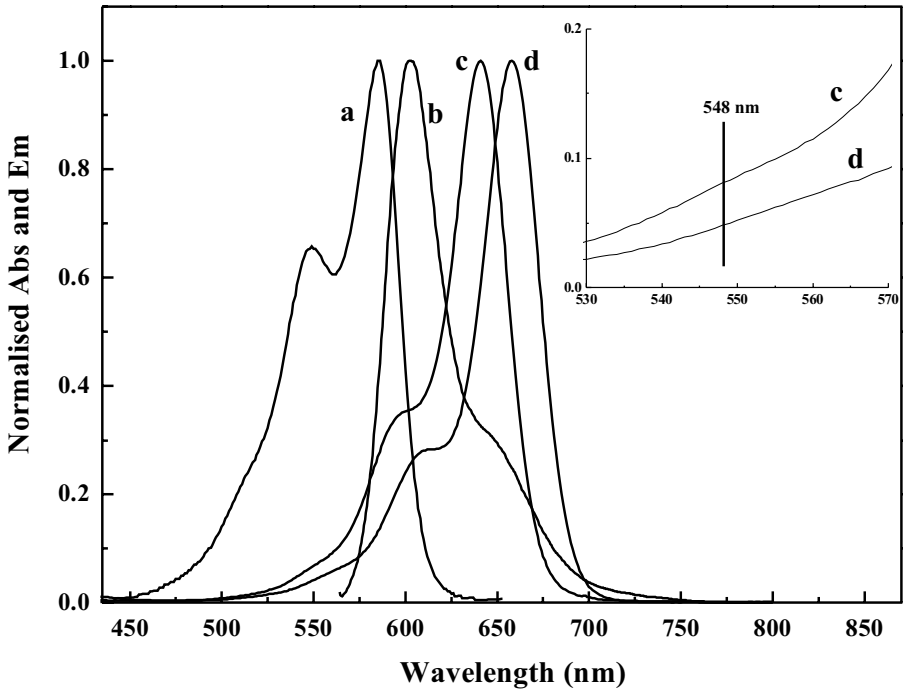

Fig. 3. Emission spectra of DYE 5 and IRIS 5NO2 at a

Figure 3.

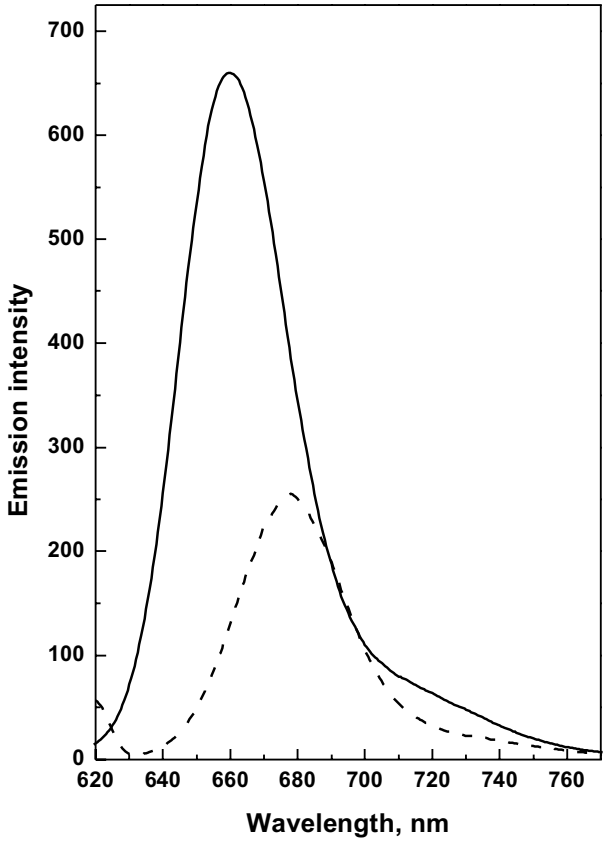

Fig.4 Quenching test.

Figure 4.